Photoelectron initial conditions for tunneling ionization in a linearly polarized laser

S. J. McNaught,* J. P. Knauer, and D. D. Meyerhofer*,†
Laboratory for Laser Energetics, University of Rochester, 250 East River Road, Rochester, New York 14623-1299
(Received 9 January 1998)

A precise measurement of the initial kinetic energy of photoelectrons born in a high-intensity, linearly polarized laser has been made in the long-pulse tunneling limit. The shape of the angular distribution of electrons outside the laser focus is related to the initial momenta the electrons gain from the field. The measurements of nonzero drift momenta for high-charge states of neon indicate tunneling ionization is occurring and agree with the predictions of the Ammosov-Delone-Krainov (ADK) model [M. V. Ammosov, N. B. Delone, and V. P. Krainov, Sov. Phys. JETP **64**, 1191 (1986)]. The validity of this model allows the value of the electron's initial kinetic energy to be limited to approximately 0.2% of its average quiver energy. [S1050-2947(98)07008-5]

PACS number(s): 32.80.Rm, 32.80.Fb

I. INTRODUCTION

The number and momentum distributions of photoelectrons observed outside an intense ionizing laser field can give insight into the ionization process occurring inside the focus. An experiment by Corkum *et al.* [1] with picosecond CO_2 laser pulses showed that an electron born (liberated from an atom by ionization) in the quasiclassical tunneling regime (the ponderomotive potential U_p is greater than the ionization potential I_p, which is greater than the photon energy ω) gains a drift, or directed, momentum at the time of ionization even if the ponderomotive, or quiver, momentum is returned to the field. These experiments gave direct evidence that tunneling ionization was occurring. The physics can be considered to occur in a two-step process known as the ''quasistatic'' or ''simpleman's'' model [1–4]. First, the electron escapes the atom by tunneling, and, second, it interacts with the external field. Quasiclassical calculations are needed for the first step, but the interaction of the free electron with the field can be treated classically [2]. Once liberated, the electron gains a drift momentum, which is determined by the phase of the laser field at the time of ionization and, depending on the length of the laser pulse, also receives a ponderomotive contribution to its final momentum [5]. The phase of the laser field at the time of ionization is determined by the ionization model. For the following discussion, linear polarization is assumed. A simple classical model, such as barrier-suppression ionization (BSI) [6], which predicts that ionization occurs only at the peak of the laser field, also predicts that the electron gains no drift momentum in a linearly polarized field. Tunneling ionization models [7,8], however, predict a significant probability of ionization occurring at off-peak phases of the optical cycle. If the electron is not born at the peak of the field, then the drift momentum is nonzero, directed along the polarization axis, and 90° out of phase with the electric field for linear polarization. It has been shown experimentally [9] that there is a significant probability of ionization at off-peak phases of the optical cycle, and, as a result, the photoelectrons gain a drift momentum directed in the polarization direction. This leads to an asymmetry in the electron number distribution in the azimuthal plane, or the plane perpendicular to the propagation direction. Here we report more precise measurements of the azimuthal angular distributions and more detailed calculations of electron initial conditions than those first reported in Ref. [9].

Keldysh [10] defined the adiabaticity parameter γ to distinguish the boundary between multiphoton and tunneling ionization. This parameter is the ratio of the electron tunneling time to the laser period and is defined as $\gamma \equiv (I_p/2U_p)^{1/2}$, where I_p is the ionization potential of the atom and $U_p = \langle F^2 \rangle / 2\omega^2$ is the ponderomotive energy (atomic units will be used throughout this paper, except in reporting energy values). Here F and ω are the amplitude and frequency of the laser field, respectively. In this experiment $\gamma < 0.1$, suggesting that ionization occurs primarily through tunneling. Ion yield [6,11] and electron spectroscopy [1,12–16] measurements have shown that when γ is less than unity, electrons are liberated primarily through tunneling, not multiphoton, ionization. Walker *et al.* [16] also made measurements of azimuthal angular distributions but not in an effort to deduce electron initial conditions. This experiment probes the initial conditions of photoelectrons in the tunneling regime, but with longer pulses and higher intensities than previous work.

In this work a high-intensity laser was used to ionize neon gas at low density, and the high-energy electron spectra as a function of the forward angle θ (relative to the **k** vector of the laser) and the azimuthal angle φ (relative to the polarization vector) were measured. The measured azimuthal distributions were used to calculate the average drift momentum and initial kinetic energy of electrons born in the creation of high charge states of neon. For linearly polarized light, a 2:1 asymmetry in the electron number distribution in the plane perpendicular to the propagation direction was observed, with more electrons detected along the direction of polarization than perpendicular to it. This distribution would be axisymmetric in the absence of an initial drift momentum because then the only contribution to the electron's final momentum would be from the ponderomotive force, which

*Present address: Department of Physics and Astronomy, University of Rochester, Rochester, NY 14627-0171.
†Present address: Department of Mechanical Engineering, University of Rochester, Rochester, NY 14627-0132.

is proportional to the intensity gradient of the laser focus [17]. The observed asymmetries must be due to a nonzero initial drift momentum and are therefore direct evidence for tunneling ionization. These experimental data are consistent with the predictions of the Ammosov-Delone-Krainov (ADK) tunneling model [8]. Furthermore, calculations of the mean initial kinetic energy of the electrons (in addition to the drift momentum predicted by the ADK model) are below the upper limit given by theoretical predictions [18].

An outline of this work is as follows: A review of the quasistatic ADK tunneling model and an analysis of the electron dynamics in a plane-wave field are presented in Sec. II. Section III includes a description of the experimental setup, the method of analysis, and the calculations of the azimuthal asymmetries. In Sec. IV the results of a relativistic Monte Carlo simulation of the experiment employing the tunneling model are reviewed and compared to the experimental data and the tunneling theory. Section V discusses calculations of the maximum initial kinetic energy predicted theoretically and allowed by the experimental data. The conclusions are presented in Sec. VI.

II. TUNNELING IONIZATION AND ELECTRON DYNAMICS

The simpleman's model was introduced as a two-step model in which the electron (1) tunnels through a Coulomb barrier that has been suppressed by a strong laser field and (2) interacts as a free electron with the external field [2]. When $I_p \gg \omega$, as is the case in this experiment, the external electric field can be assumed to be static because in the time the electron takes to tunnel through the barrier the laser field changes very slowly. Alternatively it can be said that the electron wave function reaches a steady state in a time much shorter than the laser period [2]. As a result, dc or quasistatic tunneling models, in which the ionization rate is calculated assuming a static external electric field, give a good approximation of the rate as a function of the time-varying field amplitude $F(\eta)$ (where η is the phase of the laser field). The second step of the model says that the electron trajectory can be calculated classically using the Lorentz force because the external field is much stronger than the residual Coulomb field seen by the electron.

A. Ionization models

The ionization rate of the atom as a function of the external electric field is determined by the ionization model used. Quasistatic tunneling models [1,7,8,19] give the ionization rate in the limit where the electron's Kepler period is much shorter than the laser period and assume the external field amplitude is small in comparison with the atomic field [$F \ll (2I_p)^{3/2}$, where I_p is the ionization potential]. Landau and Lifshitz calculated the result for hydrogen [19]; the expression in the work of Corkum *et al.* is valid for hydrogenic atoms [1]. The ADK theory [7,8] predicts ionization rates of complex atoms or ions by including the effective principal quantum number $n^* = Z/(2I_p)^{1/2}$ (where Z is the ion charge state), as well as orbital and magnetic quantum numbers l and m. The rate falls off exponentially as the amplitude of the electric field and is given by [7,8]

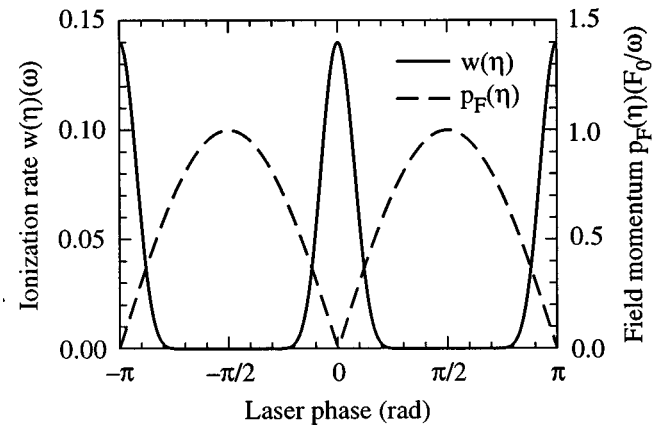

FIG. 1. ADK tunneling ionization rate $w(\eta)$ as a function of laser phase (solid curve) with ionization potential $I_p = 239$ eV, ponderomotive potential $U_p = 22$ keV, and laser intensity 2×10^{17} W/cm^2. Overlaid for comparison (dashed curve) is the magnitude of the field momentum $\mathbf{p}_F(\eta)$ in units of the maximum quiver momentum F_0/ω.

$$w(\eta) = C^2_{n^*,l^*} f_{l^*,m} I_p \left[\frac{2}{|\mathbf{F}(\eta)|} (2I_p)^{3/2} \right]^{2n^* - |m| - 1} \times \exp\left[-\frac{2}{3|\mathbf{F}(\eta)|} (2I_p)^{3/2} \right], \quad (1)$$

where $|\mathbf{F}(\eta)|$ is the amplitude of the laser's electric field. The factors $f_{l^*,m}$ and C_{n^*,l^*} are of order 1 [8]. Note that Eq. (1) is the static rate and has not been averaged over a laser period. For all rate calculations, the ground-state values for n^* and l^* are used, summed over the degenerate m states. Figure 1 shows $w(\eta)$ for electrons born in the creation of Ne^{8+} ions, for which the ionization potential is 239 eV and the peak linearly polarized electric field is 2.4 a.u. (1.2×10^{10} V/cm in real units), corresponding to a laser intensity of 2×10^{17} W/cm^2. The rate has a significant width in electric field phase, but it is most probable that the electron is born when the field is peaked at $\eta = 0, \pi, 2\pi$, etc. The probability of ionization occurring at $\eta = 0$ is 1000 times larger than that at $\eta = \pi/4$.

The simple model of barrier-suppression ionization (BSI) [6] can be considered the classical limit of the tunneling model. BSI assumes, like the tunneling model, that the laser period is much longer than the electron's Kepler period (i.e., the quasistatic limit), but unlike ADK it allows the electron to be born only at the peak of the electric field. Once the field ''suppresses'' the Coulomb barrier low enough, the electron can escape. The critical field for ionization in atomic units is found to be [6]

$$F_{\text{crit}} = \frac{I_p^2}{4Z}, \quad (2)$$

where Z is the charge on the residual ion. For the BSI model, the rate in Fig. 1 would be delta functions at $\eta = 0, \pi, 2\pi$, etc. Equation (1) can be integrated over time to calculate the threshold field for ionization in the ADK model. Figure 2 is a plot of the fraction of atoms in a given charge state (Ne^{7+}) ionized as a function of time, given a 2-ps full width at half

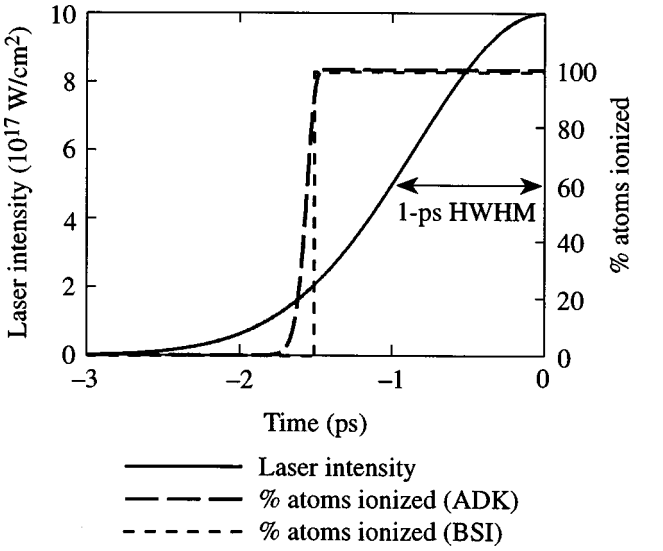

FIG. 2. Fraction of Ne^{7+} ions ionized as a function of time, according to (i) the ADK tunneling model (the long-dashed curve) and (ii) the classical BSI model (the short-dashed curve). This calculation was made for a 2-ps FWHM laser pulse with a peak intensity of 1×10^{18} W/cm^2. The laser intensity is overlaid for comparison (solid curve). The threshold intensity for ionization is about the same for both models and is approximately 2×10^{17} W/cm^2.

maximum Gaussian laser pulse with peak intensity 1×10^{18} W/cm^2. The long-dashed line is the fraction ionized according to the ADK theory, and the short-dashed line shows the same for the BSI theory. The solid curve is the laser intensity overlaid for comparison. The curve for the BSI theory is a step function because the model assumes all of the available atoms are ionized when the peak electric field reaches the critical field $F_{\rm crit}$. Despite the differences between the models, the ADK curve shows that just over half of the atoms are ionized by the time the laser field reaches the BSI threshold intensity, which is about 2×10^{17} W/cm^2. Therefore the field seen by most of the photoelectrons at the time of ionization is about the same for both models.

B. Electron dynamics and drift momentum

After ionization occurs, the electron dynamics are determined by calculating the Lorentz force exerted on the free electron in the external field. Several mechanisms give rise to electron drift once it is freed from the atom. Besides the drift momentum due to the electron's initial phase in the field and any initial kinetic momentum, the electron can also gain a directed drift momentum from the ponderomotive force. These three sources of drift will be discussed below.

The simpleman's model assumes that upon ionization the Coulombic effects of the residual ion or other ions can be ignored because the laser field is much stronger than the Coulomb field and the oscillation amplitude of the electron is much larger than the distance over which the atomic potential is appreciable [2]. In this experiment, the electron oscillation amplitude in the external field is over 1000 times greater than the size of the parent ion. The electron, once freed into the field, may have some initial kinetic momentum, perhaps due to residual momentum from its orbit. A second initial condition is the phase of the laser within the optical cycle at the time of ionization, which gives the electron another component of drift momentum. Both of these conditions define one conserved quantity, the canonical momentum. For simplicity consider a linearly polarized, plane-wave field in the velocity gauge with the vector potential and electric field

$$\mathbf{A}(\eta)=-\hat{\mathbf{x}}\,\frac{cF_0\sin\,\eta}{\omega}$$

and

$$\mathbf{F}(\eta)=\hat{\mathbf{x}}F_0\cos\,\eta, \tag{3}$$

where $\eta\equiv\omega t-\mathbf{k}\cdot\mathbf{r}$ is the Lorentz invariant laser phase and F_0 is the peak electric field, which is proportional to the square root of the laser intensity [20]. The canonical momentum is the difference of the initial kinetic momentum $\mathbf{p}_k(\eta_0)$ and the vector potential at the time of ionization $\mathbf{A}(\eta_0)$

$$\mathbf{P}_{\rm can}=\mathbf{p}_k(\eta_0)-\frac{1}{c}\,\mathbf{A}(\eta_0), \tag{4}$$

where η_0 is the time of ionization as a phase. The field is assumed to be planar, so $\mathbf{p}_k$, $\mathbf{A}$, and $\mathbf{P}_{\rm can}$ are all defined in the plane of polarization and have no longitudinal components. Since the canonical momentum is conserved, Eq. (4) shows that the electron gains an effective drift momentum from the field

$$\mathbf{p}_d(\eta_0)\equiv\mathbf{p}_k(\eta_0)+\hat{\mathbf{x}}\,\frac{F_0\sin\,\eta_0}{\omega}=\mathbf{p}_k(\eta_0)+\mathbf{p}_F(\eta_0), \tag{5}$$

which is just the sum of the initial kinetic momentum $\mathbf{p}_k(\eta_0)$ and what is called the ''field momentum'' $\mathbf{p}_F(\eta_0)$ [18]. For the moment it is assumed that the initial kinetic momentum $\mathbf{p}_k(\eta_0)$ is negligible, so the drift momentum is just equal to the field momentum. The field momentum $\mathbf{p}_F(\eta_0)$, which arises from the electron's initial condition in the field, is in the direction of the electric field and is nonzero if $\eta_0\neq0$, π, 2π, etc.

For the tunneling model, ionization occurs over a finite phase angle so some electrons are born with significant field momentum. Overlaid on Fig. 1 is the value of the field momentum as a function of phase in units of F_0/ω, the maximum quiver momentum. Since $\mathbf{p}_F(\eta_0)$ is 90° out of phase with the electric field, as the phase increases from $\eta_0=0$, $\mathbf{p}_F(\eta_0)$ also increases. The classical BSI theory predicts that the field momentum is always identically zero because the electron is always born at the peak of the field. The ionization rate $w(\eta)$ given by Eq. (1) and as shown in Fig. 1 has a significant width for linear polarization, which implies that the electrons have a nonzero initial root-mean-square (rms) field momentum. The rms field momentum $p_{F,\rm rms}$ is defined by

$$p_{F,\rm rms}^2=\frac{F_0^2}{\omega^2}\,\frac{\int_0^{\pi/2}(\sin^2\eta)w(\eta)d\eta}{\int_0^{\pi/2}w(\eta)d\eta}. \tag{6}$$

For the case shown in Fig. 1, the rms field momentum as defined by Eq. (6) is $0.22\,F_0/\omega$.

Since experimental measurements of the electron energy are made outside the laser focus, ponderomotive effects must also be considered. The ponderomotive force accelerates the electron as it traverses the focus and therefore is important in determining the electron's final momentum. The ponderomotive potential U_p is equal to the average quiver energy of the electron in the field, and the corresponding force $\mathbf{F}_p$ is proportional to the gradient of the laser intensity [17]:

$$\mathbf{F}_p = -\frac{1}{2c^2}\nabla\langle\mathbf{A}^2\rangle \propto -\nabla I. \tag{7}$$

If the duration of the laser pulse is long enough, the quiver energy U_p of the electron is converted into directed kinetic energy, and the electron is ejected from the focus. The electrons can be thought to be accelerating down the intensity ''hill'' created by the laser field. If the spatial intensity distribution in the laser focus is axisymmetric, then the ponderomotive force is also axisymmetric, and electrons cascade down the hill isotropically [21]. A schematic of this effect is shown in Fig. 3. If the initial field momentum $\mathbf{p}_F(\eta_0)$ is zero, then equal numbers of electrons are observed at all angles in the azimuthal plane, as illustrated in Fig. 3(a). If, however, $\mathbf{p}_F(\eta_0)$ is nonzero, then electrons are preferentially directed along the x axis, as shown in Fig. 3(b). The limit in which the laser pulse is long enough such that the ponderomotive energy from the field is fully converted into directed kinetic energy is called the ''long-pulse'' limit [22]. In the short-pulse limit, the electron gains the drift energy $\mathbf{p}_d(\eta_0)$ from the initial condition at the time of ionization, and, depending on the direction of the drift momentum and the phase of the electron when the field turns off, may gain some directed momentum from ponderomotive effects [23].

Unlike several short-pulse limit investigations of electron spectra in the multiphoton and tunneling regimes [1,12–16,24], the electrons in this experiment gain the full ponderomotive energy from the field. The ponderomotive force adds a symmetric component to the final azimuthal angular distribution outside the focus. Figure 4 shows how the azimuthal distribution of electrons varies from the short- to long-pulse limit. The curve at the bottom of Fig. 4 is the ratio of the major (x) to minor (y) axes of the azimuthal distribution predicted using computer simulations of ADK ionization (described in more detail in Sec. IV). Three examples of the azimuthal distributions are also shown at the top of Fig. 4 as polar plots, with the x and y axes indicated. The parameters used are those for electrons born in the creation of Ne^{8+} ions, for which $\gamma = 0.07$ and $U_p = 22$ keV. Note that in the case of very short laser pulses (10 fs), almost all of the electrons are directed along the x (polarization) direction, but as the pulse duration crosses into the long-pulse limit, the ponderomotive force begins making a significant contribution to the final azimuthal distribution. When a 100-fs pulse duration is used, the number asymmetry is about 2:1 and remains that value as the pulse duration increases. For pulses longer than 100 fs, the electrons gain the full ponderomotive energy, and thus the shape of the distribution is unchanged as a function of pulse duration. Despite the fact that ponderomotive effects decrease the number asymmetry, the number asymmetry remains a very sensitive measure of the electrons' initial condition.

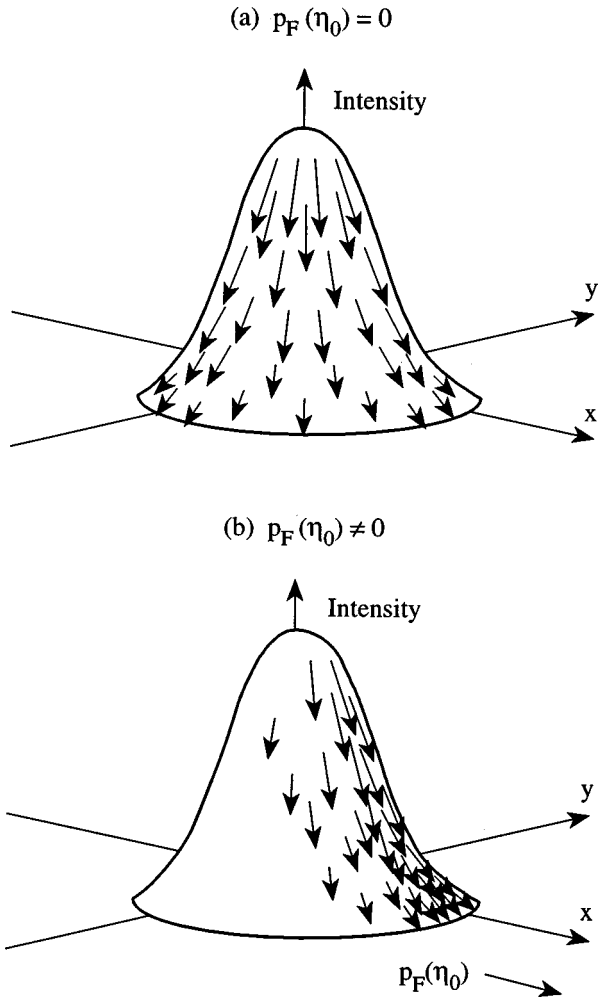

FIG. 3. Schematic of the intensity surface that electrons encounter when born in a high-intensity laser focus. (a) Electrons born with zero field momentum $\mathbf{p}_F(\eta_0)$ cascade down the ponderomotive ''hill'' isotropically, gaining the full ponderomotive energy as they exit the focus. (**b**) Electrons born with an initial field momentum $\mathbf{p}_F(\eta_0)$ are ejected from the focus preferentially in the electric field (x) direction and also gain the full ponderomotive energy.

The investigation of ionization dynamics described in this paper has been carried out in the long-pulse regime because very high intensities, up to 10^{18} W/cm^2, are needed to ionize neon to the eighth charge state. To observe electrons from this charge state in the short-pulse regime where ponderomotive effects are minimized, laser intensities of 10^{18} W/cm^2 would be required in a pulse shorter than 50 fs. More importantly, it can be seen from Fig. 4 that very precise measurement of the laser pulse width would be required in a short-pulse experiment because, in this regime, the number asymmetry is extremely sensitive to the pulse duration.

III. EXPERIMENTAL SETUP AND RESULTS

A. Experimental apparatus

In the experiment, the distribution of photoelectrons as a function of energy E, forward angle θ, and angle φ in the plane perpendicular to the propagation direction was measured for electrons produced in the creation of high charge states of neon. θ is defined relative to the laser's propagation

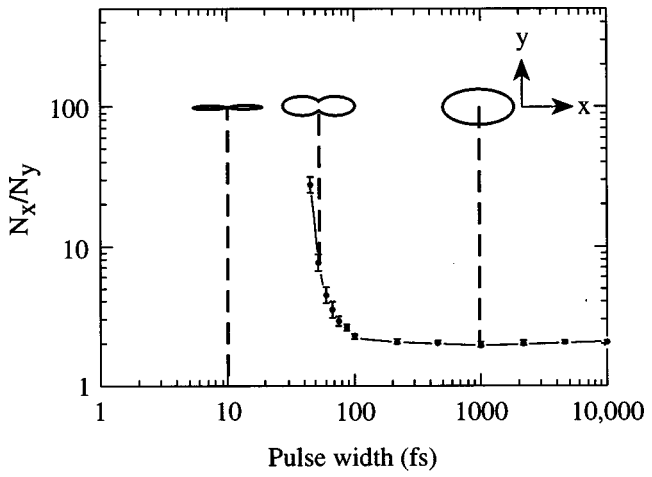

FIG. 4. A plot of the number asymmetry N_x/N_y of the azimuthal angular distribution of electrons as a function of laser pulse duration for electrons with $I_p=239$ eV and $U_p=22$ keV. Electrons ejected from laser pulses longer than 100 fs are in the long-pulse limit and therefore gain the full ponderomotive energy. At the top of the figure are polar plots of the azimuthal distribution at laser pulse durations of 10 fs, 50 fs, and 1 ps. The electric field in these plots is in the x (horizontal) direction.

direction, and φ is defined relative to the polarization axis. Electrons with energies up to 30 keV were observed. Previous measurements with circularly polarized laser pulses showed photon momentum transfer to the ejected electrons [25] and effects of the mass shift of electrons oscillating in the laser field [26]. The measurement of the electron distributions as a function of both energy and θ is necessary to resolve the closely spaced energy peaks of the upper charge states of neon. The relation between the electron's final kinetic energy E and forward scattering angle θ is given, to a good approximation, by [23,25,27,28]

$$\theta=\tan^{-1}\sqrt{2c^2/E}, \tag{8}$$

where c is the speed of light. This relation remains valid regardless of the electron's initial momentum. Measurement of the electron distributions perpendicular to the **k** vector exclusively would neglect the forward momentum gained by the electrons [25].

A schematic of the experimental setup is shown in Fig. 5. A 1.054-μm, 2-ps laser using chirped-pulse amplification [29] was focused with an aspheric $f/3$ lens to a 5-μm ($1/e^2$ radius) focal spot and a peak laser intensity up to 1×10^{18} W/cm^2. Shot-to-shot measurements of the laser energy and pulse duration were made with a pin diode and single-shot autocorrelator, respectively. A one-time measurement of the focal spot radius was made by imaging the laser focus after the beam exited the vacuum chamber. Neon gas at a pressure of 1×10^{-3} Torr in a background of 5×10^{-9} Torr was used to minimize space charge effects. Laser ionization provided electrons that escaped the focus in a time much shorter than the pulse duration. No electrons were observed with energies much above the sum of the ponderomotive and drift energies for a tunneling process, which ensured that no collective processes were occurring. The absence of collective plasma processes was also indicated by the linear dependence of the electron signal on the neon gas pressure up to several mTorr. The electron energy spectra were measured as a function of azimuthal angle φ by leaving the spectrometer stationary and rotating the laser field polarization using a half-wave plate. The shot-to-shot variation in the laser's pointing accuracy at the focus was ±1.2 μm and did not change when the half-wave plate was rotated.

The spectrometer [25,30] consists of an electromagnet to select electron energy and a detector composed of a scintillator coupled to a photomultiplier tube. The energy window

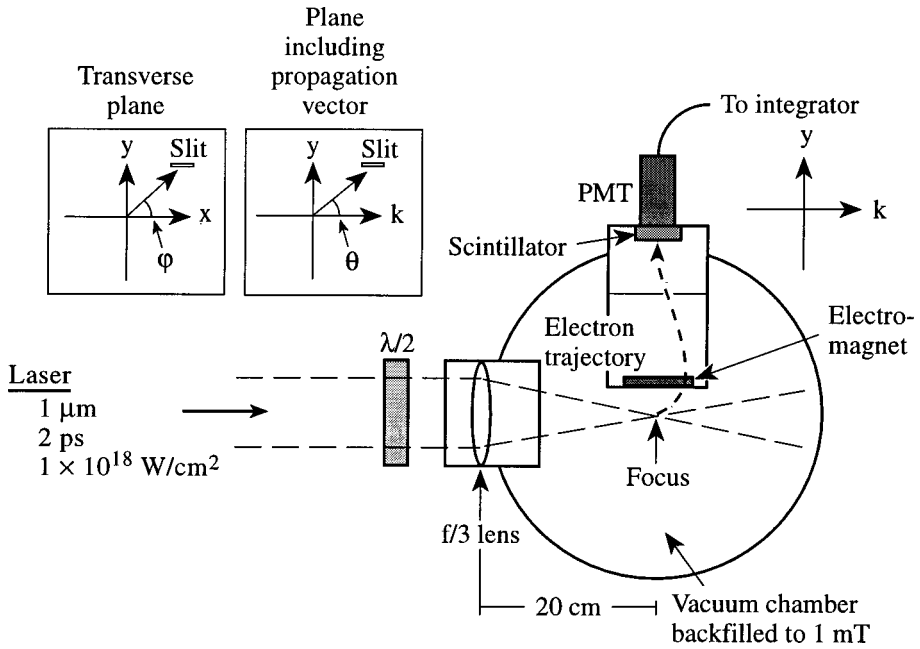

FIG. 5. Schematic of the experimental apparatus. A 1-μm, 2-ps laser is focused to intensities up to 1×10^{18} W/cm^2 in a vacuum chamber backfilled to 1 mTorr of neon. Photoelectrons from ionized atoms escape the laser focus, pass through a slit in a magnetic spectrometer, and are detected by a scintillator coupled to a PMT.

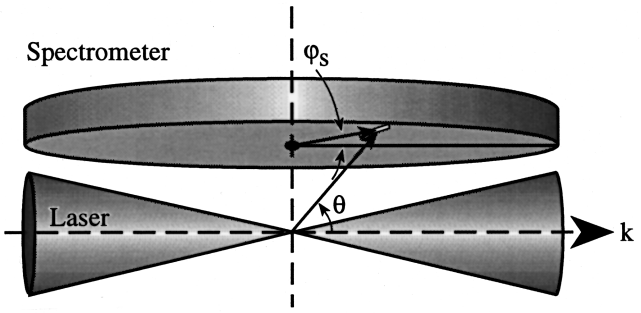

FIG. 6. The geometry of the laser focus in relation to the bottom of the spectrometer and the slit is shown. The forward angle θ is determined from the angle of rotation φ_s of the spectrometer.

of the spectrometer was varied by changing the magnetic field in the 2-mm gap of the steering magnet. The field in the gap was known in a range from 10 to 600 G from a calibration using a Hall probe. An energy calibration of the spectrometer using a beam of monoenergetic electrons gave an energy resolution of $\Delta E/E = 30\%$ FWHM [30]. The spectrometer's signal was not reliable below an electron energy of 2.5 keV. The distribution of electrons as a function of θ was measured by rotating the entire spectrometer about the cylindrical axis that passes through the laser focus at 90° to the laser axis. Figure 6 shows the base of the spectrometer and the relation of the slit to the laser focus. The angle θ is determined relative to the angle of rotation φ_s of the spectrometer by the relation $\cos\theta = (\cos\varphi_s)/\sqrt{2}$. The angular resolution of the spectrometer is $\Delta\theta = \pm 1.5°$, and the angular acceptance in the azimuthal plane is $\Delta\varphi = 3°$. Peak signal-to-noise ratios of 1000 to 1 were obtained with this setup [30].

B. Measurement of energy spectra

The energy spectra measured by this spectrometer differ from those seen before [1,12–16] for two reasons: First, as discussed above, the electrons in this experiment are born in the long-pulse tunneling regime and, therefore, gain the full ponderomotive energy from the field. The energy spectrum associated with electrons from a particular charge state is expected to be centered on the ponderomotive energy U_p. Figure 7 shows typical energy spectra for electrons born in (a) the short-pulse and (b) the long-pulse tunneling regimes, according to a Monte Carlo computer simulation (described in detail in Sec. IV). In Fig. 7(a) is the familiar short-pulse energy spectrum, with the maximum signal at a kinetic energy of zero, falling off to an energy of $2U_p$. This spectrum was generated for electrons born in the creation of Ne^+ in a 1.054-μm laser field with a peak intensity of 2×10^{15} W/cm^2 and a pulse duration of 100 fs. The laser pulse passes before these electrons have time to gain any significant ponderomotive energy, and therefore the maximum energy they attain is $2U_p$, given by the drift momentum shown in Eq. (5). This spectrum is integrated over the forward angle θ. Figure 7(b) shows electron spectra for electrons born in the creation of charge states Ne^{6+}, Ne^{7+}, and Ne^{8+}. The signal from charge states below Ne^{6+} was omitted for clarity. These electrons were born in a laser field with the same parameters as the experiment described in this paper: a peak intensity of 7×10^{17} W/cm^2 and a pulse length of 2 ps. In such a field the electrons have enough time to gain the full ponderomotive energy from the field, and this contribution to the final kinetic energy overwhelms that of the drift energy that determined the shape of the spectra in the short-pulse regime. Electrons in this regime can also attain energies up to $2U_p$, but the signal at $2U_p$ is orders of magnitude smaller than that at $1U_p$. Three spectra were ''measured'' at forward angles of $\theta = 79°$, 82°, and 85°, with an angular acceptance angle of $\Delta\theta = \pm 1.5°$. Note that there are three peaks evident in the spectra, each with an energy corresponding roughly to the ponderomotive energy U_p predicted by the ADK theory (indicated on the graph).

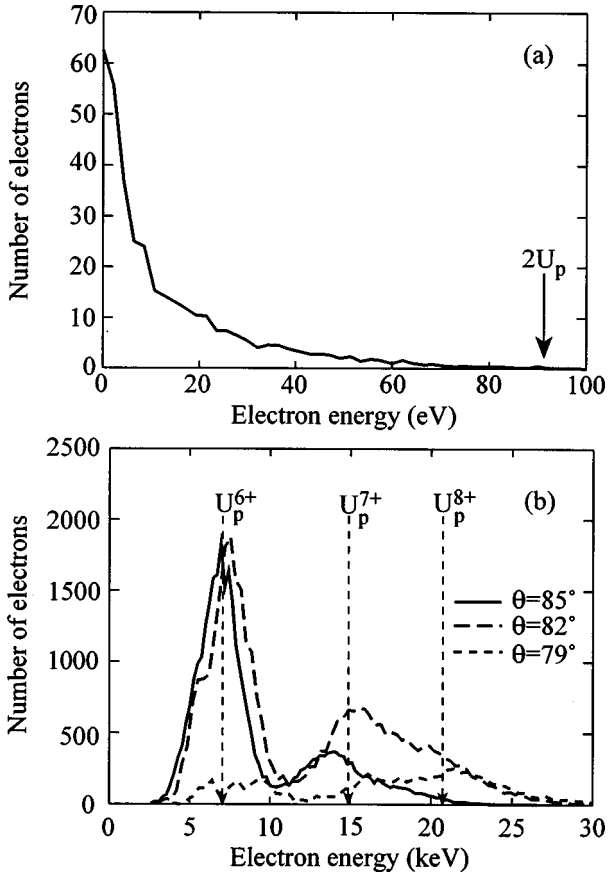

FIG. 7. Simulated electron energy spectra for electrons born in the tunneling regime in (a) the short-pulse and (b) the long-pulse limits. Electrons in (a) were liberated in the creation of Ne^+ by a 1.054-μm laser with a peak intensity of 2×10^{15} W/cm^2 and a pulse duration of 100 fs. The signal falls off to a maximum energy of $2U_p$. Electrons in (b) were liberated in the creation of Ne^{6+}, Ne^{7+}, and Ne^{8+} by a 1.054-μm laser with a peak intensity of 7×10^{17} W/cm^2 and a pulse duration of 2 ps. The signal from ions below Ne^{6+} is omitted for clarity. The three spectra shown were measured at forward angles of $\theta = 85°$ (solid curve), $\theta = 82°$ (dashed curve), and $\theta = 79°$ (dotted curve). Each peak corresponds to the ponderomotive energy U_p predicted by the ADK model for that charge state.

The second difference of the spectra measured here from short-pulse tunneling spectra is the higher final kinetic energies measured and unique response of the spectrometer used. Figure 7(b) shows that the spectra observed as a function of forward angle θ changes in accordance with Eq. (8). The

spectrum at $\theta=85°$ shows electrons with energies lower than those at $\theta=79°$, and most of the signal seen at $\theta=85°$ is due to Ne^{6+} electrons, whereas most of the signal at $\theta=79°$ is due to Ne^{8+} electrons. As the forward angle θ decreases, the average energy observed increases; thus it is expected that relatively more signal will be observed from higher charge states than lower charge states as θ decreases. For electrons with final energies greater than 1 keV, Eq. (8) and these calculations show that measurement of spectra as a function of θ as well as energy is crucial in determining the contributions of the different charge states to the final spectra. The contribution of the forward momentum to the electron trajectories was insignificant in previous experiments [1,12,14–16] that measured much lower final energies.

Measurements of energy spectra of electrons from high charge states of neon were made to determine the energies E_{peak} and angles θ_{peak} at which the signal peaked as a function of energy and angle θ. Energy spectra were measured at azimuthal angles φ of 0° and 90° and at forward angles θ of 78° through 90°. Measurements of the energy spectra both parallel and perpendicular to the polarization axis were made to determine if and how the number asymmetry varied as a function of energy. Figure 8(a) shows a typical energy spectrum; this one was measured at $\theta=82°$, both parallel and perpendicular to the polarization direction. This spectrum shows three distinct peaks for the $\varphi=0°$ spectrum. When multiple-Gaussian least-squares fits were made to each energy spectrum, it was found that peaks appeared in the spectra at roughly the same energies regardless of the forward angle setting. To determine the values of θ_{peak}, the peak electron number fit value from the energy fits was plotted as a function of angle θ for each peak in the energy spectra. Subsequent Gaussian fits to these angular spectra then gave values for θ_{peak} at $\varphi=0°$ and $\varphi=90°$. Figure 8(b) shows the forward angular spectrum of the highest-energy electrons observed at $\varphi=0°$ and $\varphi=90°$. This spectrum represents electrons in an energy window from about 19 to 26 keV. The measured angle θ_{peak} agrees with the measured final kinetic energy E_{peak} according to Eq. (8) at both $\varphi=0°$ and $\varphi=90°$. The values of E_{peak} from the three highest-energy peaks observed in the energy spectra correspond to the average expected final energy for electrons born in the creation of Ne^{6+}, Ne^{7+}, and Ne^{8+} according to the ADK model. Measurement of electron energy exclusively at $\theta=90°$ would have given spectra with inaccurately low energies. The spectrometer could not resolve any difference between the value of E_{peak} at $\varphi=0°$ and that at $\varphi=90°$, so an initial drift momentum could not be calculated from the energy data. Most importantly, an approximately 2:1 asymmetry in electron number was observed for all three charge states. This asymmetry is used below to estimate the initial drift momentum.

The correlation between the signal observed and the charge state primarily responsible for those electrons is made by the spectrometer's ability to resolve peaks in the signal as a function of both energy and forward angle θ. Figure 9 is a contour polar plot of the signal observed, where the distance from the origin represents the energy observed and the angle from the horizontal axis represents the forward angle θ. Electrons ejected at $\theta=90°$ (those with energies below 1 keV) would appear on the vertical axis. The scale of the graph is

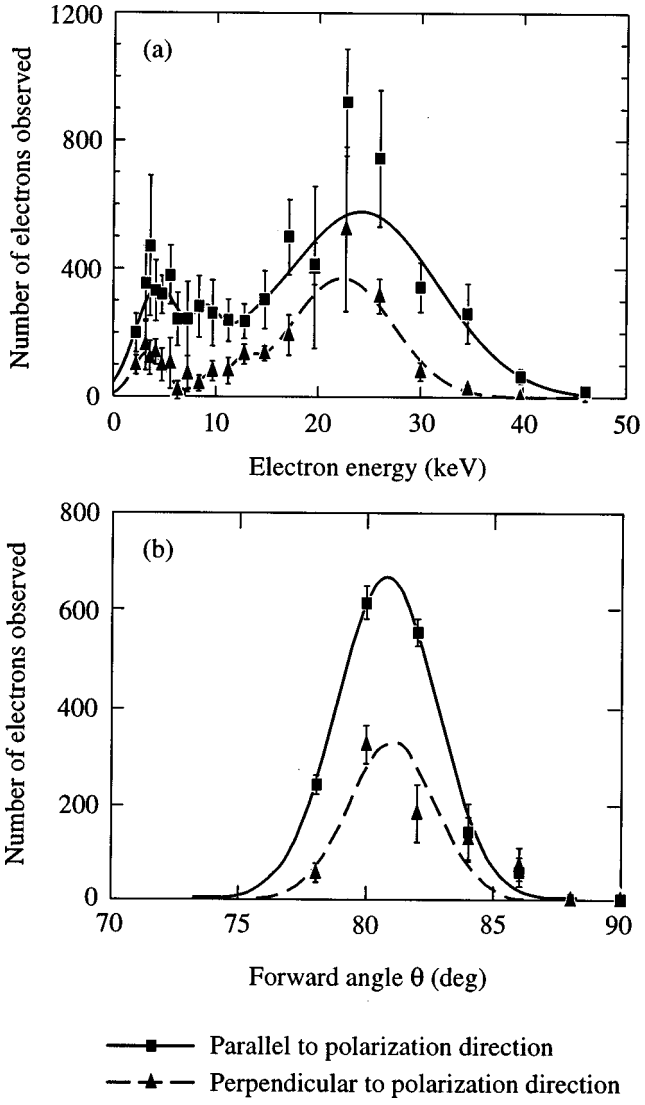

FIG. 8. (a) The energy spectra of neon photoelectrons from a linearly polarized laser focus seen at a forward angle $\theta=82°$ and azimuthal angles $\varphi=0°$ (solid curve) and $\varphi=90°$ (dashed curve). Note the 2:1 asymmetry in electron number. (b) The distribution of electrons produced in the creation of Ne^{8+} ions as a function of forward angle θ at azimuthal angles $\varphi=0°$ and $\varphi=90°$.

exaggerated in the horizontal direction so that the contours can be discerned. The contribution of each of the three highest-energy peaks to the total signal in (E,θ) space is plotted as contours at 50%, 75%, and 90% of the maximum signal observed. Also plotted is the relation between the final energy E and forward angle θ given by Eq. (8) (dashed curve) and the predicted value of $(E_{\text{peak}},\theta_{\text{peak}})$ for electrons produced in the creation of Ne^{6+}, Ne^{7+}, and Ne^{8+} according to the ADK model (squares). The experimental data agree with the ADK values for all three charge states. This two-dimensional spectrum was generated by scanning through the values of the multiple-Gaussian fits to the experimental energy spectra with a regular energy step size and fitting Gaussians as a function of angle θ. The width of the signal attributed to Ne^{8+} electrons is larger than that of Ne^{6+} because the energy resolution of the spectrometer is proportional to the energy measured. The dotted curves are lines of equal energy. The signal characteristic of short-pulse elec-

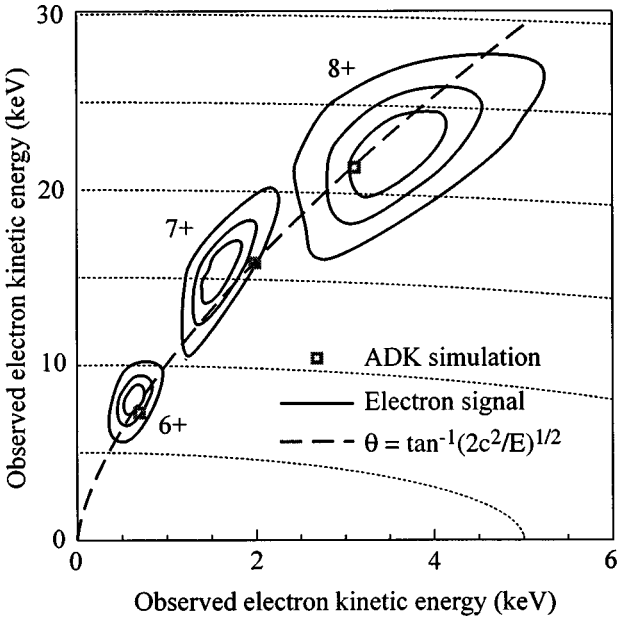

FIG. 9. Contour polar plot of the observed electron signal. The distance from the origin represents the measured electron energy E, and the angle from the horizontal axis represents the forward angle θ. The contribution of each of the three highest-energy peaks to the total signal as a function of energy and angle is plotted as contours at 50%, 75%, and 90% of the maximum signal observed. Also plotted is the relation between E and θ given by Eq. (8) (dashed curve) and the predicted value of (E_{peak}, θ_{peak}) for electrons produced in the creation of Ne^{6+}, Ne^{7+}, and Ne^{8+} according to the ADK model (squares). The experimental data agree with the ADK values for all three charge states.

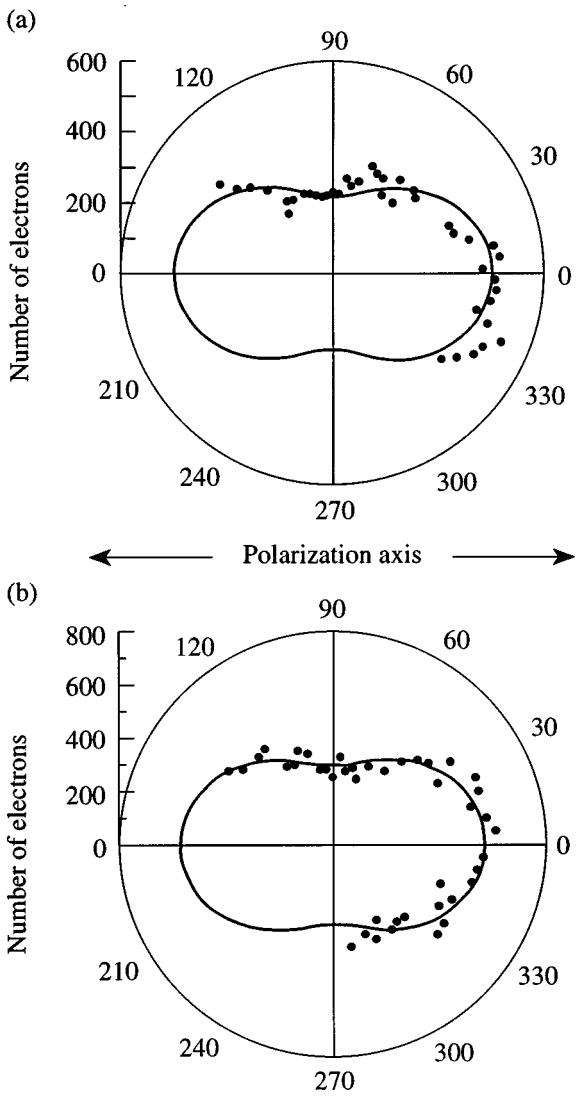

FIG. 10. The azimuthal angular spectrum of electrons seen at the peak energy and peak forward angle for electrons produced in the creation of (a) Ne^{6+} and (b) Ne^{8+} electrons. In both cases a 2:1 number asymmetry is observed, with more electrons seen along the polarization axis.

tron spectra as illustrated in Fig. 7(a) could not be separated into contributions from different charge states if the atoms were multiply ionized. This experiment, however, shows that in the long-pulse tunneling regime and with this spectrometer the signal at its maximum values can be primarily attributed to electrons coming from a particular charge state. Previous ion-yield experiments with this laser system have shown the presence of high charge states of neon at the intensities used in this experiment, and that the yields of these ions agree with the predictions of the ADK model [6].

C. Measurement of azimuthal spectra

Previous experiments used retarding potentials to measure the drift energy of the electrons by calculating the difference in electron energy parallel and perpendicular to the polarization direction [1,13]. Because the drift momentum is directed along the polarization direction, the *number*, as well as *energy*, of electrons observed along the polarization direction is greater than that seen perpendicular to it. In this experiment the number of electrons as a function of azimuthal angle was measured in addition to energy spectra measurements. The azimuthal angular distribution has been found to be a more sensitive measure of the initial kinetic momentum of the electrons than the azimuthal energy distribution, as will be shown below.

The azimuthal angular distributions were measured by keeping the spectrometer at the E_{peak} and θ_{peak} values determined from the energy spectra and by rotating the $\lambda/2$ wave plate through about 90°, thereby rotating the polarization vector through 180°. Four shots were taken at each angle setting, and before averaging, the signal obtained from each shot was normalized appropriately (see Appendix). Figure 10 shows polar plots of the azimuthal distributions measured for electrons born in the creation of (a) Ne^{6+} and (b) Ne^{8+}. More electrons are observed along the polarization direction than perpendicular to it, as predicted theoretically. To determine the ratio N_x/N_y, the ratio of the number of electrons seen in the direction parallel to the polarization direction to that seen perpendicular to the polarization direction, a function of the form $N=a+b\cos(2\varphi)$ was fit to the data. This functional form has no theoretical basis but was chosen empirically as it fit the azimuthal distributions best among a set of simple functions tested. From the data, $N_x/N_y=(a+b)/(a-b)$ was found to have the values 2.08 ± 0.13, 2.06 ± 0.08, and 1.92 ± 0.08 for electrons produced in the creation of Ne^{6+}, Ne^{7+}, and Ne^{8+}, respectively. The errors in N_x/N_y were determined by propagating the errors in the fit param-

eters a and b. These data give a mean error of 4.7% in the ratio, which is an improvement over the data presented in Ref. [9].

IV. MONTE CARLO SIMULATION

An idealized computer simulation of the experiment was performed to understand the effect of the initial drift momentum on the number asymmetry observed outside the focus. An analytical solution for the azimuthal distribution was impossible because of complications raised by the complex electric field of a Gaussian focus and broadening of the energy spectra caused by electrons being born at different locations in the focal volume. These calculations are used to compare the drift momentum observed experimentally to that predicted theoretically by the ADK tunneling model.

The fully relativistic Monte Carlo simulation from Ref. [30] has been modified to determine the relation between the number ratio N_x/N_y and the electron's initial drift momentum. To assess the effect of the drift momentum on the final trajectories, the first simulations presented use classical BSI ionization and the trajectories are calculated as a function of imposed initial drift momentum in the polarization direction. This initial drift momentum has a distribution of arbitrary width $p_{d,\mathrm{rms}}$ and Gaussian shape. Each atom was placed randomly within the focal volume for a given peak laser intensity, and a linearly polarized laser pulse with a Gaussian spatial and temporal profile was propagated over the atom. Each atom was ionized when the laser field reached the BSI threshold given by Eq. (2), and the electron was released into the field with the initial drift momentum. After ionization the fully relativistic Lorentz equations of motion for the trajectories were solved for each of the 25 000 atoms simulated per charge state. Each simulated electron represented approximately 50 electrons in the experimental laser focus. The measured 5-μm beam waist and 2-ps laser pulse of the laser system were used in the simulation. The peak intensity in the simulation was set to the average peak intensity measured in the laboratory, which, depending on the experiment, was between 7×10^{17} and 1×10^{18} W/cm^2. Once the electrons were well outside the laser focus, a second simulation convolved the trajectories of the electrons through the magnetic spectrometer. By ''positioning'' the detector at some forward angle θ and azimuthal angle φ, the number of electrons could be measured in the same manner as in the experiment. Data obtained from this simulation were analyzed in the same manner as described above for the experimental data. Energy spectra as a function of forward angle θ were analyzed to determine E_{peak} and θ_{peak} for each charge state, and then a continuous azimuthal distribution was ''measured'' at these values for each charge state. The same function $N=a+b\cos(2\varphi)$ was fit to these azimuthal distributions as was used for the experimental data. Figure 11 shows the number asymmetry N_x/N_y from the simulation for electrons produced in the creation of Ne^{8+}, as a function of the initial rms momentum width $p_{d,\mathrm{rms}}$ of the simulated electrons. The shaded region represents the confidence interval given by the experimental value of N_x/N_y. $P_{d,\mathrm{rms}}$ is given in units of F_0/ω. These calculations estimate the experimental rms width of the initial drift momentum distribution to be $23.8\pm2.1\%$, $23.2\pm0.7\%$, and $22.8\pm1.0\%$ of F_0/ω for

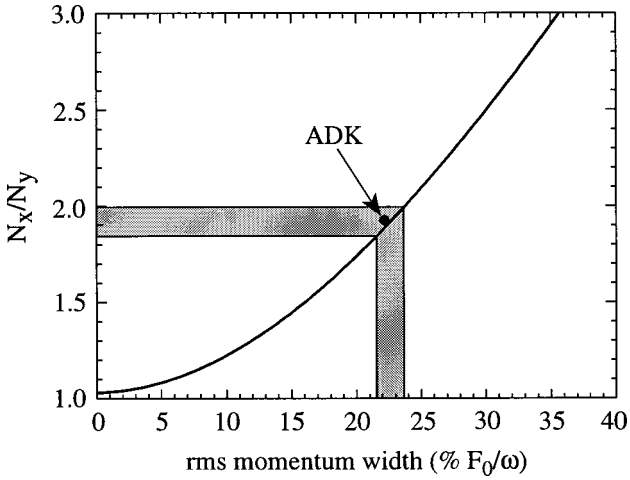

FIG. 11. Number asymmetry N_x/N_y observed versus the rms momentum width, given Ne^{8+} electrons according to the Monte Carlo simulation. The shaded region represents the confidence interval of the experimental value of N_x/N_y. The values of N_x/N_y and the rms value of the field momentum $p_{F,\mathrm{rms}}$ predicted by the ADK tunneling theory agree with the experimental data.

electrons produced in the creation of Ne^{6+}, Ne^{7+}, and Ne^{8+}, respectively. The errors in $p_{d,\mathrm{rms}}$ were determined graphically by propagating the error in N_x/N_y to the $p_{d,\mathrm{rms}}$ axis as shown in Fig. 11. These momenta correspond to an average drift energy that is about 9% of the ponderomotive energy U_p for all charge states considered.

The initial drift momenta values inferred from the data are in good agreement with those predicted by the ADK tunneling model [8] when the electrons have zero initial kinetic momentum $\mathbf{p}_k(\eta_0)$. To determine the drift momentum width according to the ADK model, the Monte Carlo simulation was modified to calculate ionization rates according to the tunneling theory instead of the simpler classical model. For each simulated electron, the equation

$$C(\eta_0)=1-\exp\left[-\int_{-\infty}^{\eta_0} w(\eta)\,d\eta\right] \tag{9}$$

was solved for η_0, the time of ionization, where $C(\eta_0)$, the fraction of atoms ionized by the time η_0, was incremented continuously from zero to one. This calculation determined the phase of birth η_0 for each electron. A plot of the number of electrons as a function of η_0 (modulo 2π) yielded a curve similar to that given in Fig. 1. Each electron was then released into the field at the time η_0 with zero initial kinetic momentum $\mathbf{p}_k(\eta_0)$. The second stage of the simulation was identical to that described above. Figure 12 shows the azimuthal angular distribution generated by the ADK simulation overlaid on the experimental data for Ne^{8+} electrons from Fig. 10(b). The only free parameter between the two distributions is an overall scaling factor. It can be seen that the experimental and simulated data agree well, as the curves fit to the two data sets are barely discernible.

From the ADK ionization rate $w(\eta)$ the rms value of the field momentum $p_{F,\mathrm{rms}}$ was calculated according to Eq. (6) and from the Monte Carlo simulation the values E_{peak}, θ_{peak}, and N_x/N_y for each charge state were calculated. The tunneling theory gave values for $p_{F,\mathrm{rms}}$ of 22.7, 22.7, and 22.2 %

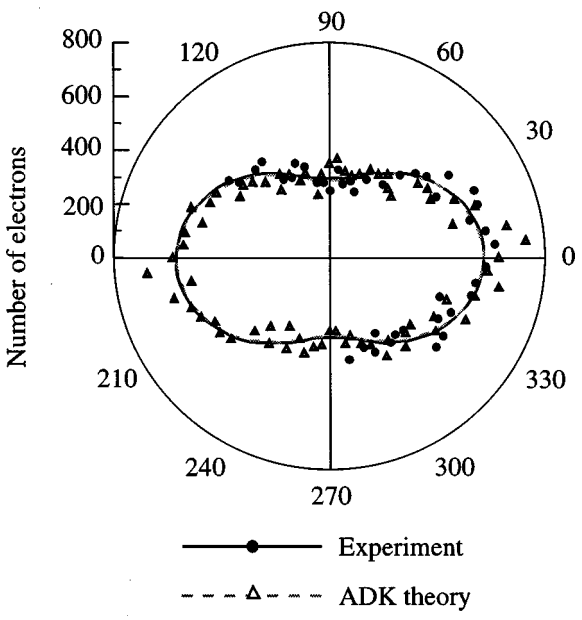

FIG. 12. The azimuthal angular spectrum of electrons measured experimentally (solid circles and solid line) and calculated numerically by the ADK Monte Carlo simulation (triangles and dashed line). The fits to both data sets overlap and are practically indiscernible. The only free-fitting parameter between these spectra is an overall scaling factor.

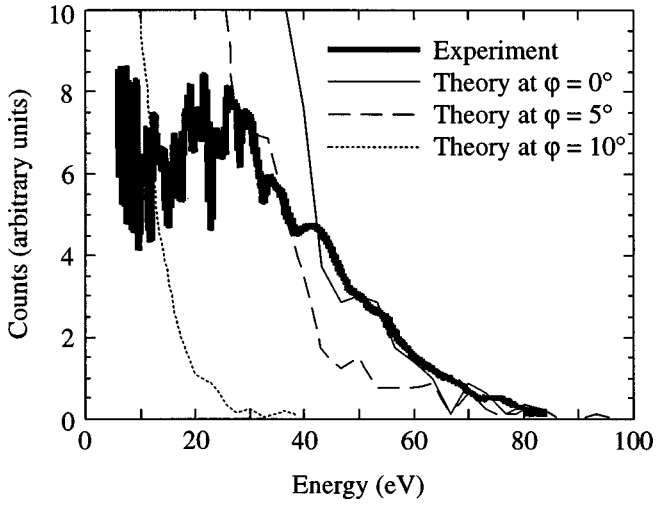

FIG. 13. Energy spectra of electrons born in the creation of He^+ ions as a function of angle φ in the azimuthal plane from Mevel *et al.* [12] and the ADK Monte Carlo simulation. These spectra were calculated under the experimental conditions of Mevel *et al.* [12], whose spectrum is shown as the heavy curve. The simulated spectra shown are measured at (i) $\varphi=0°$ (solid line), (ii) $\varphi=5°$ (dashed line), and (iii) $\varphi=10°$ (dotted line). The amplitude and width of the spectra are strong functions of the angle φ, with almost all of the electrons being ejected along the polarization direction ($\varphi=0°$).

of F_0/ω for Ne^{6+}, Ne^{7+}, and Ne^{8+} electrons, respectively. The value for Ne^{8+} differs mostly because this electron is the last available in the second atomic shell of neon. The calculated values of N_x/N_y were 2.06, 2.04, and 1.91, respectively, when the function $N=a+b\cos(2\varphi)$ was fit to the simulated ADK data. The value of N_x/N_y obtained from the fit to the simulation data shown in Fig. 12 is shown on Fig. 11 versus the ADK value of $p_{F,\mathrm{rms}}$. These values agree with the experimental asymmetries given above for all three charge states. Table I summarizes the experimental and ADK values of the peak final electron energy and drift momentum for each charge state. As given in Table I, E_{peak} is the average of the measured values of the peak energy at each forward angle θ, and the error is the standard deviation of these values. Because the field momentum is a strong function of laser phase at the time of ionization, these calculations show that the ADK model well represents the physics occurring inside the laser focus at the time of ionization.

The Monte Carlo simulation employing the tunneling model can also be used to simulate an experiment by Mevel *et al.* [12] given some assumptions about their experimental setup. The researchers measured spectra of electrons born in the ionization of various noble gases (from Xe to He) using a linearly polarized 100-fs, 617-nm laser. This was done to show the transition of the spectra from the multiphoton regime, in which the Keldysh parameter $\gamma\gg1$, to the tunneling regime, in which $\gamma\ll1$ [12]. An energy spectrum of electrons from He^+ that was measured using a time-of-flight spectrometer extended to 90 eV [12], even though the ponderomotive energy for these electrons is only about $U_p=50$ eV and the initial drift energy is about $\mathbf{p}_F(\eta_0)^2/2=10$ eV. Because the experiment was done in the short-pulse limit, the electrons' final energy is due primarily to the drift momentum directed along the polarization direction, as well as any additional momentum in this direction due to ponderomotive effects, and is very sensitive to the laser's peak intensity and pulse width. As a result the azimuthal distribution should resemble the one shown on the far left (top) of Fig. 4, with almost no signal perpendicular to the polarization direction. Figure 13 shows the He^+ energy spectra produced by the Monte Carlo simulation at several angles φ under the experimental conditions of Ref. [12]. The experimental data are overlaid for comparison. It is clear from the simulation that there is a strong dependence of the spectrum's mean energy and overall amplitude on the azimuthal angle. Only the tail of the spectrum at $\varphi=0°$ agrees with the experimental spectrum.

TABLE I. The experimental and predicted ADK values of the energy of peak electron signal E_{peak} for electrons produced in the creation of Ne^{6+} to Ne^{8+} ions are given. The last two columns give the rms values of the experimental drift momentum and ADK field momentum for each charge state.

	E_{peak} (expt)	E_{peak} (ADK)	$p_{d,\mathrm{rms}}$ (expt)	$p_{F,\mathrm{rms}}$ (ADK)
Ne^{6+}	7.7±0.7 keV	7.3 keV	23.8±2.1% F_0/ω	22.7% F_0/ω
Ne^{7+}	15.3±1.8	15.8	23.2±0.7%	22.7%
Ne^{8+}	22.2±0.9	21.5	22.8±1.0%	22.2%

An experimental investigation of the energy spectrum's evolution as a function of the angle φ in the azimuthal plane under these conditions would be enlightening.

V. INITIAL KINETIC MOMENTUM

In the previous sections it has been assumed that the initial kinetic momentum $\mathbf{p}_k(\eta_0)$ of the photoelectrons is zero, and therefore by Eq. (5) the drift momentum is equal to the field momentum. Under this assumption, the data agreed well with the predictions of the Monte Carlo simulation employing the ADK ionization model; therefore $\mathbf{p}_k(\eta_0)$ must be small in comparison to the electron's final momentum.

According to Goreslavsky *et al.* [18], the probability of ionization as a function of initial kinetic momentum is greatest when the initial kinetic momentum is zero, but there is a nonzero probability of the electron being born with some initial kinetic momentum. As a result there is a characteristic width associated with the ionization rate as a function of $\mathbf{p}_k(\eta_0)$. Also, Goreslavsky *et al.* predict that it is not possible for the electron to be born with initial kinetic momentum in the direction of the instantaneous electric field; for the case of linear polarization this is always the x direction [18]. The initial kinetic momentum $\mathbf{p}_k(\eta_0)$ can just as likely be in the propagation (z) direction as in the direction perpendicular to the electric field (the y direction). Reference [18] predicts that the spread in the initial kinetic energy is given nominally by $\Delta K_{\rm th}(\eta_0)=F_0/2(2I_p)^{1/2}$ and that this initial energy must be larger than the photon energy $[\Delta K_{\rm th}(\eta_0)>\omega]$ and smaller than the ionization potential $[I_p>\Delta K_{\rm th}(\eta_0)]$. The spread $\Delta K_{\rm th}(\eta_0)$ in initial kinetic energy satisfies the uncertainty principle $\Delta K_{\rm th}(\eta_0)=1/\tau_{\rm tr}$, where $\tau_{\rm tr}$ is the duration of the electron's quantum transition (i.e., the tunneling time) [18].

To determine the upper bounds on the initial kinetic energy implied by the experimental data, the ADK Monte Carlo simulation was modified to allow for a Gaussian distribution of initial kinetic momentum $\mathbf{p}_k(\eta_0)$ in the x, y, or z directions *in addition* to the ADK field momentum. To determine the limits on $p_{k,x}(\eta_0)$ and $p_{k,y}(\eta_0)$, the components of $\mathbf{p}_k(\eta_0)$ in the x and y directions, the number asymmetry N_x/N_y was plotted as a function of the rms value of $p_{k,x}(\eta_0)$ and $p_{k,y}(\eta_0)$. If $p_{k,x}(\eta_0)\neq 0$ and $p_{k,y}(\eta_0)=0$, then more electrons are directed along the x axis than the y axis, and N_x/N_y increases. If $p_{k,x}(\eta_0)=0$ and $p_{k,y}(\eta_0)\neq 0$, then N_x/N_y decreases. Figure 14(a) is a plot of the number asymmetry versus the rms value of $p_{k,x}(\eta_0)$ (the solid curve) or $p_{k,y}(\eta_0)$ (the dashed curve). All momenta are expressed in units of F_0/ω. The value of the asymmetry at $p_{k,x}(\eta_0)=p_{k,y}(\eta_0)=0$ is that predicted by the unmodified ADK simulation. The lines leading from the vertical axis represent the limits of the experimental data for Ne^{8+} electrons. These data limit $p_{k,x}(\eta_0)$ to 3.5% of F_0/ω and $p_{k,y}(\eta_0)$ to 3.7% of F_0/ω. This corresponds to initial kinetic energy upper bounds $K_x(\eta_0)\equiv p_{k,x}^2(\eta_0)/2$ and $K_y(\eta_0)$ of only 47 and 54 eV, respectively for Ne^{8+} electrons, which represents only 0.2% of these electrons' final kinetic energy. The maximum initial kinetic energies $K_x(\eta_0)$ and $K_y(\eta_0)$ for all three charge states are listed in Table II. These data suggest some possible spread in the initial kinetic momentum in the x (polarization) direction not predicted by theory [18].

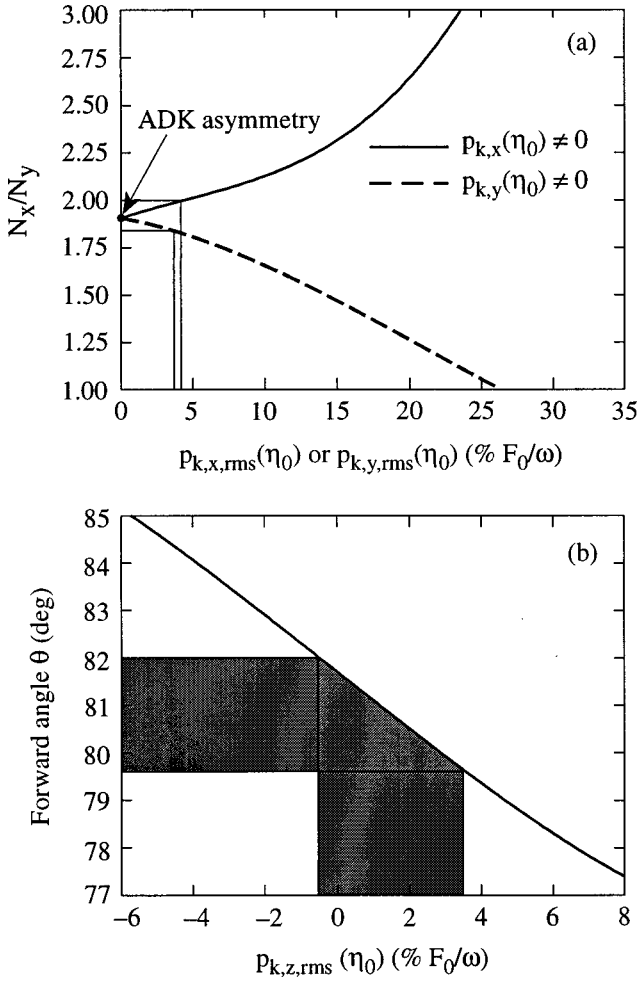

FIG. 14. (a) Number asymmetry given by the modified ADK Monte Carlo simulation for Ne^{8+} electron as a function of (i) $p_{k,x,\rm rms}(\eta_0)$ (solid curve) and (ii) $p_{k,y,\rm rms}(\eta_0)$ (dashed curve). From these data the upper limits on the value of both $p_{k,x}(\eta_0)$ and $p_{k,y}(\eta_0)$ can be determined and are both less than 4% of F_0/ω. (b) The peak forward angle $\theta_{\rm peak}$ as a function of $p_{k,z,\rm rms}(\eta_0)$ in units of F_0/ω for Ne^{8+} electrons. The initial kinetic momentum $p_{k,z}(\eta_0)$ is determined to be less than 3.5% of F_0/ω.

The limits placed on $p_{k,z}(\eta_0)$, the z component of $\mathbf{p}_k(\eta_0)$, were calculated using the values of $\theta_{\rm peak}$ measured in the laboratory. From the ADK Monte Carlo simulation with $p_{k,z}(\eta_0)\neq 0$, the peak forward angle $\theta_{\rm peak}$ for each charge state as a function of the rms momentum width in the z direction was calculated, with $p_{k,x}(\eta_0)=0$ and $p_{k,y}(\eta_0)=0$. Figure 14(b) shows the upper limits placed on $p_{k,z}(\eta_0)$ by the experimental value of $\theta_{\rm peak}$ for Ne^{8+} electrons. The limit of $p_{k,z}(\eta_0)$ on the positive side corresponds to an initial kinetic energy of only 47 eV. The maximum initial kinetic energy $K_z(\eta_0)$ given by the experimental data for all three charge states appears in Table II. The sensitivity of $\theta_{\rm peak}$ in limiting the initial conditions is about the same as that of the number asymmetry in the azimuthal plane.

On average, for all orientations and charge states, the initial kinetic energy is limited to only 0.18% of the electron's average quiver energy at the time of ionization. Assuming accuracy of the ADK model, the uncertainty in the initial

TABLE II. The ionization potential I_p, experimental maximum initial kinetic energy in the x, y, and z directions, estimated uncertainty in the initial kinetic momentum, and theoretical uncertainty in the initial kinetic momentum is given for electrons produced in the creation of Ne^{6+} to Ne^{8+} ions.

		Maximum initial kinetic energy				
	I_p	$K_x(\eta_0)$ (expt)	$K_y(\eta_0)$ (expt)	$K_z(\eta_0)$ (expt)	$\Delta K_{\text{expt}}(\eta_0)$	$\Delta K_{\text{th}}(\eta_0)$ (Ref. [18])
Ne^{6+}	158 eV	4.4 eV	8.3 eV	6.1 eV	11 eV	5.1 eV
Ne^{7+}	207	34	7.1	57	67	6.8
Ne^{8+}	239	47	54	47	86	7.5

kinetic momentum is estimated by adding in quadrature the calculated maximum values in each of the three dimensions:

$$[\Delta K_{\text{expt}}(\eta_0)]^2 = K_x^2(\eta_0) + K_y^2(\eta_0) + K_z^2(\eta_0). \quad (10)$$

For Ne^{6+} electrons, $\Delta K_{\text{expt}}(\eta_0)$ is only 11 eV, compared to an ionization potential $I_p = 158$ eV and an observed final energy of 7.7 keV. Table II gives the estimated uncertainty $\Delta K_{\text{expt}}(\eta_0)$ and the theoretical uncertainty $\Delta K_{\text{th}}(\eta_0)$ [18] for each charge state. Although $\Delta K_{\text{expt}}(\eta_0)$ approaches $\Delta K_{\text{th}}(\eta_0)$ only for Ne^{6+} electrons, in all cases the measured values are between the limits given by the photon energy (1.2 eV) and the ionization potential, shown in Table II for each ion.

The sensitivity of this measure of the initial kinetic energy is illustrated by the results given by looking at the *energy* asymmetry instead of the *number* asymmetry: Using experimental values of E_x/E_y—the ratio of the peak electron energy seen along the polarization direction to that seen perpendicular to it—an average limit on the initial kinetic energy $\mathbf{p}_k(\eta_0)^2/2$ of 14% of the electron's average quiver energy U_p was calculated. The sensitivity of the number asymmetry method is of the order of 100 times greater than that of the energy asymmetry method under these experimental conditions.

VI. SUMMARY AND CONCLUSIONS

The simpleman's model [2] states that atoms or ions in a high-intensity laser field are ionized primarily through tunneling when the electron's tunneling time is much shorter than the laser period (the adiabatic or low-frequency limit). Theoretically there is a finite probability of the electron being born with a nonzero initial kinetic momentum $\mathbf{p}_k(\eta_0)$, but the ionization rate is peaked for zero initial kinetic momentum [18]. In addition, there is a significant probability of the electron being born at off-peak phases of the electric field in the tunneling regime. If the electron is not born at the peak of the electric field, it immediately gains a component of drift called the field momentum $\mathbf{p}_F(\eta_0)$, which for linear polarization is in the polarization direction and 90° out of phase with the electric field. A third mechanism for electron drift is due to the ponderomotive force, which, if the laser pulse is long enough, introduces a component of directed momentum along the spatial intensity gradient of the focus.

We have made a precise measurement of the drift momentum $\mathbf{p}_d(\eta_0)$ of high-energy electrons born in a linearly polarized, high-intensity laser focus in the long-pulse tunneling regime. Good agreement was obtained between calculations of the rms drift momentum from the ADK model and drift momentum derived from the experimental number asymmetry. The limits placed on the initial kinetic momentum relative to the ionization potential and ponderomotive energy are smaller than any measured previously and agree with those predicted by theory, which states that $\omega < \Delta K(\eta_0) < I_p \ll U_p$ [18].

Experiments that have investigated the transition from multiphoton to tunneling ionization [12,16] have shown experimentally that Stark-induced resonances spaced by the photon energy, which are clearly evident when $\gamma > 1$, are washed out at the onset of the tunneling regime when γ falls to less than 1. The conclusion from these experiments [12,16] and ion-counting experiments [6,11] that tunneling ionization is occurring in this regime is strengthened by the results of the experiment presented here, which show the effect of the field momentum on the azimuthal distribution of electrons.

These measurements provide important support for the interpretation of experimental results in high-order harmonic generation and direct double ionization. In the former case, knowledge of the magnitude of the initial kinetic momentum, as well as the drift momentum, can place a more precise constraint on the cutoff energy of the high-harmonic plateau [31]. Knowledge of both the initial kinetic $\mathbf{p}_k(\eta_0)$ and field $\mathbf{p}_F(\eta_0)$ momenta can also help describe the process of rescattering of the electron on the residual ion or other ions [4].

The upper limits on the initial kinetic momentum $\mathbf{p}_k(\eta_0)$ can be further reduced by measuring the values of θ_{peak} and N_x/N_y for each charge state at several different ellipticities of laser polarization, including circular polarization. This will allow an even tighter constraint to be put on the initial kinetic momentum by fitting a curve to number asymmetry data points as a function of laser ellipticity.

ACKNOWLEDGMENTS

The authors gratefully acknowledge the contributions of J. H. Eberly, S. P. Goreslavsky, and C. I. Moore. This work was supported by the National Science Foundation. Additional support was provided by the U.S. Department of Energy Office of Inertial Confinement Fusion under Cooperative Agreement No. DE-FC03-92SF19460, the University of Rochester, and the New York State Energy Research and Development Authority. The support of the U.S. DOE does not constitute an endorsement by the DOE of the view expressed in this work.

APPENDIX: NORMALIZATION OF THE ELECTRON SIGNAL

The signal measured by the magnetic spectrometer and PMT must be properly normalized on a shot-to-shot basis to

account for fluctuations in laser intensity at the focus. In this experiment, the signal detected by the PMT is directly proportional to the energy of electrons striking the scintillator as well as to the focal volume [30]. The former is compensated by dividing the signal by the electron energy corresponding to the calibration performed on the electromagnet. Compensating for the fluctuation of laser intensity is more difficult. The focal volume is the volume within the laser focus within which the intensity exceeds the threshold intensity for ionization of the atom or ion at the peak of the laser pulse [32]. If the laser focus is assumed to be Gaussian, then the time-independent intensity distribution takes the form

$$I(\mathbf{r}) = I_0 \left(\frac{w_0}{w_z} \right)^2 \exp\left[-2 \left(\frac{\mathbf{r}}{w(z)} \right)^2 \right], \tag{A1}$$

where w_0 is the $1/e^2$ beam waist at focus (here about 5 μm),

$$w(z) \equiv w_0 \sqrt{1 + z^2/z_0^2}, \tag{A2}$$

and z_0 is the Rayleigh range [33]. Given a threshold intensity of $I_{\rm th}$ and a peak intensity of I_0, it can be shown that the volume enclosed by the maximum radius and axial position at which ionization can occur is [32]

$$V(I_0, I_{\rm th}) = \frac{2\pi w_0^2 z_0}{9 I_{\rm th}^{3/2}} \left\{ (5I_{\rm th} + I_0)(I_0 - I_{\rm th})^{1/2} - 6 I_{\rm th}^{3/2} \tan^{-1}\left[\left(\frac{I_0 - I_{\rm th}}{I_0} \right)^{1/2} \right] \right\}. \tag{A3}$$

The threshold intensity $I_{\rm th}$ was determined in the laboratory by setting the spectrometer at energy $E_{\rm peak}$ and forward angle $\theta_{\rm peak}$ at which the maximum signal was observed and plotting the signal measured at each shot as a function of the laser intensity. Equation (A3) was fit to these data in order to determine the value of $I_{\rm th}$. Each shot taken in the azimuthal distribution measurement with intensity I_i was normalized by a factor $N_i = V(I_0, I_{\rm th})/V(I_i, I_{\rm th})$, where I_0 was set to the average laser intensity measured over the course of the experiment. For all of the azimuthal scans, the peak laser intensity I_0 was about 8×10^{17} W/cm^2. The experimental value of $I_{\rm th}$ agreed roughly with that predicted by the tunneling model for all three charge states; for example, $I_{\rm th}$ was measured for Ne^{8+} electrons to be $(2.3 \pm 0.5) \times 10^{17}$ W/cm^2, and it is predicted theoretically to be 2×10^{17} W/cm^2.

[1] P. B. Corkum, N. H. Burnett, and F. Brunel, Phys. Rev. Lett. **62**, 1259 (1989).

[2] H. B. van Linden van den Heuvell and H. G. Muller, in *Cambridge Studies in Modern Optics 8: Multiphoton Processes*, edited by S. J. Smith and P. L. Knight (Cambridge University Press, New York, 1988), p. 25; H. G. Muller, Comments At. Mol. Phys. **24**, 355 (1990).

[3] T. F. Gallagher, Phys. Rev. Lett. **61**, 2304 (1988).

[4] P. B. Corkum, Phys. Rev. Lett. **71**, 1994 (1993).

[5] S. P. Goreslavsky, M. V. Federov, and A. A. Kil'pio, Laser Phys. **5**, 1020 (1995).

[6] S. Augst *et al.*, Phys. Rev. Lett. **63**, 2212 (1989); S. Augst *et al.*, J. Opt. Soc. Am. B **8**, 858 (1991).

[7] A. M. Perelemov, V. S. Popov, and M. V. Terent'ev, Zh. Eksp. Teor. Fiz. **50**, 1393 (1966) [Sov. Phys. JETP **23**, 924 (1966)].

[8] M. V. Ammosov, N. B. Delone, and V. P. Krainov, Zh. Eksp. Teor. Fiz. **91**, 2008 (1986) [Sov. Phys. JETP **64**, 1191 (1986)].

[9] S. J. McNaught, J. P. Knauer, and D. D. Meyerhofer, Phys. Rev. Lett. **78**, 626 (1997).

[10] L. V. Keldysh, Zh. Eksp. Teor. Fiz. **47**, 1945 (1964) [Sov. Phys. JETP **20**, 1307 (1965)].

[11] F. Yergeau, S. L. Chin, and P. Lavigne, J. Phys. B **20**, 723 (1987).

[12] E. Mevel *et al.*, Phys. Rev. Lett. **70**, 406 (1993).

[13] P. Monot *et al.*, Phys. Rev. Lett. **70**, 1232 (1993).

[14] U. Mohideen *et al.*, Phys. Rev. Lett. **71**, 509 (1993).

[15] B. Walker *et al.*, Phys. Rev. Lett. **73**, 1227 (1994).

[16] B. Walker *et al.*, Phys. Rev. Lett. **77**, 5031 (1996).

[17] T. W. B. Kibble, Phys. Rev. Lett. **16**, 1054 (1966).

[18] S. P. Goreslavsky and S. V. Popruzhenko, Laser Phys. **7**, 700 (1997).

[19] L. D. Landau and E. M. Lifshitz, *Quantum Mechanics*, 2nd rev. ed. (Pergamon, New York, 1965), p. 276.

[20] A useful conversion formula for the electric field is F (V/cm) $= 27.5[I(\text{W/cm}^2)]^{1/2}$.

[21] J. H. Eberly, J. Javanainen, and K. Rzazewski, Phys. Rep. **204**, 331 (1991).

[22] P. Agostini *et al.*, Phys. Rev. A **36**, 4111 (1987).

[23] P. B. Corkum, N. H. Burnett, and F. Brunel, in *Atoms in Intense Fields*, edited by M. Gavrila (Academic Press, Boston, 1992), Supplement 1.

[24] R. R. Freeman and P. H. Bucksbaum, J. Phys. B **24**, 325 (1991).

[25] C. I. Moore, J. P. Knauer, and D. D. Meyerhofer, Phys. Rev. Lett. **74**, 2439 (1995).

[26] D. D. Meyerhofer *et al.*, J. Opt. Soc. Am. B **13**, 113 (1996).

[27] J. N. Bardsley, B. M. Penetrante, and M. H. Mittleman, Phys. Rev. A **40**, 3823 (1989).

[28] H. R. Reiss, J. Opt. Soc. Am. B **7**, 574 (1990).

[29] Y.-H. Chuang *et al.*, J. Opt. Soc. Am. B **8**, 1226 (1991).

[30] C. I. Moore, Ph.D. thesis, University of Rochester, 1995.

[31] J. L. Krause, K. J. Schafer, and K. C. Kulander, Phys. Rev. Lett. **68**, 3535 (1992).

[32] S. J. Augst, Ph.D. thesis, University of Rochester, 1991.

[33] P. W. Milonni and J. H. Eberly, *Lasers* (Wiley, New York, 1988), p. 484.